

SonoSAMTrack - Segment and Track Anything on Ultrasound Images

Hariharan Ravishankar, Rohan Patil, Vikram Melapudi, Stephan Anzengruber, Parminder Bhatia, Kass-Hout Taha, Pavan Annangi

GE HealthCare

Abstract. In this paper, we present SonoSAM - a promptable foundational model for segmenting objects of interest on ultrasound images. Fine-tuned exclusively on a rich, diverse set of objects from $\approx 200k$ ultrasound image-mask pairs, SonoSAM demonstrates state-of-the-art performance on 8 unseen ultrasound data-sets, outperforming competing methods by a significant margin on all metrics of interest. SonoSAM achieves average dice similarity score of $> 90\%$ on almost all test data-sets within 2-6 clicks on an average, making it a valuable tool for annotating ultrasound images. We also extend SonoSAM to 3-D (2-D +t) applications and demonstrate superior performance making it a valuable tool for generating dense annotations from ultrasound cine-loops. Further, to increase practical utility of SonoSAM, we propose a two-step process of fine-tuning followed by knowledge distillation to a smaller footprint model without comprising the performance. We present detailed qualitative and quantitative comparisons of SonoSAM with state-of-the-art methods showcasing efficacy of SonoSAM as one of the first reliable, generic foundational model for ultrasound.

Keywords: Foundational models, Ultrasound Imaging, Semantic Segmentation.

1 Introduction

In many of the AI-powered ultrasound imaging applications, semantic segmentation of objects is of fundamental importance. While, popular DL architectures like U-Net[1] achieve state-of-the-art (SOTA) performance, the biggest bottleneck is in getting annotated data. Obtaining exact contour markings of objects of interest in ultrasound, mandates involvement of experts with clinical knowledge, is often tedious and time-consuming. The issue is exacerbated in 3-D or 2-D+t volumes, where getting dense contour marking for multiple objects across all the frames for a subject alone is extremely challenging.

Recently, AI-powered tools have become popular for assisting object annotation in natural images. By learning on large number of image-mask pairs in the order of billions [3], these models learn the concept of “objectness” and function as generic, class-agnostic object segmentors. Models like FocalClick [2], Segment anything (SAM) [3] have advanced “promptable” segmentation, where user supplies prompts and models will automatically delineate objects of interest. The different types of user prompts are scribbles [7,8], bounding box [9,10], extreme points [11], clicks (most explored owing to ease of use), texts and images [17].

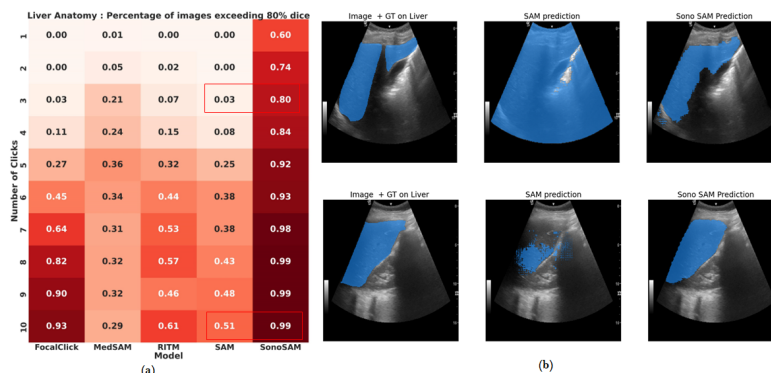


Fig. 1: a) Distribution of number of clicks versus percentage of images on which average Dice overlap exceeds 80%, b) Example images and predictions after 2 clicks for SAM and proposed method of SonoSAM.

Major breakthrough in click-based segmentation was presented in RITM [18], using iterative sampling to generate clicks during training [19]. FocalClick [2] utilized localized inference strategy to further improve accuracy. SimpleClick [23] explored the use of vision transformers for interactive segmentation. Segment anything model (SAM) [3] extended this to multiple prompts, and trained on massive data (1 billion images) to enable several mainstream applications including zero-shot segmentation. SAM has emerged as the gold standard for promptable segmentation owing to its success in multiple domains [3].

Utility of SAM[3] in medical imaging has been assessed recently in [26,27,28]. In an extensive experimental study [26], the authors find that while SAM obtains reasonable performance on different modalities, the performance is the poorest on ultrasound. This behavior is to be expected since ultrasound possesses unique characteristics like presence of scan cone, poor image quality and unique texture with speckles. Fig. 1a shows inefficiency of SAM on liver images, where after 3 clicks, SAM achieves 80% or more dice in only 3% of images. In a more striking failure, even after 10 clicks, SAM can achieve $> 80\%$ dice in roughly half the number of images. An example image shown in Fig. 1b, depicts that after two clicks, SAM segments the scan cone which is of scarce utility to the clinician.

An early attempt at developing a foundational model for medical imaging was proposed in MedSAM [27], where authors finetuned SAM on 200K image-mask pairs obtained from 11 modalities including ultrasound, using only bounding box prompts. While MedSAM outperforms SAM on first prompt, it is still extremely inadequate, fails consistently with more clicks, and is often poorer than SAM on ultrasound data. This has prompted the community to speculate that either modality-specific or organ-specific models [28] are the optimal granularity for foundation models to be of practical utility in the clinical community. With this motivation, we present SonoSAM: ultrasound modality-specific segment anything foundation model trained with a set of 200K ultrasound image-mask pairs.

The key contributions of our paper are as follows:

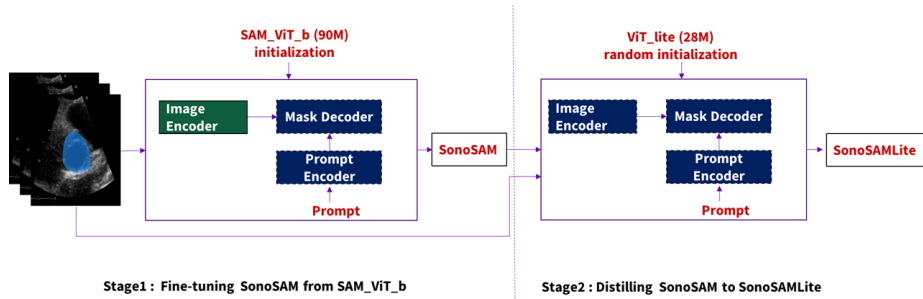


Fig. 2: Two stage process of building SonoSAM and SonoSAMLite. - Green boxes depict frozen weights and blue boxes capture fine-tuned weights.

- a first of its kind foundational model exclusively for ultrasound images enabling promptable segmentation,
- extensions to 3-D (2-D + t) use-cases with SOTA tracking methods,
- demonstration of state-of-the-art performance on 8 unseen ultrasound datasets,
- development of a deployable low footprint model with knowledge distillation.

2 Technical Details

2.1 Architecture

For semantic segmentation, there are essentially two types of backbones in practice - 1) hierarchical backbone: predominantly CNN-based [1] which learn coefficients that exploit local image content, use downsampling layers and aggregation to capture global information. 2) Plain backbone: boosted by the success of vision transformers (ViT) in other problems, segmentation architectures without pyramidal feature aggregation architecture have become popular. In SimpleClick [4], authors proposed architecture with plain backbone of various sizes - ViT_b, ViT_l, ViT_h which correspond to base, large and huge vision transformers with 90M, 300M and 600M parameters respectively. These architectures were further used in building SAM [3] models. Owing to the success of these backbones, we fine-tuned SonoSAM models starting from ViT_b model of SAM [3].

2.2 Fine-tuning strategies

a) Partial Fine-tuning - Domain specific decoder: SAM models are made up of 3 sub-blocks namely Image encoder, prompt encoder and mask decoder. In terms of number of parameters, image encoder is heaviest containing almost $> 90\%$ of parameter count. In the first stage (Fig. 2), we freeze the image encoder and fine-tune the prompt encoder and mask decoder on ultrasound images. Since, SAM has been trained on billions of natural images, we hypothesize that the image encoder of SAM should have reasonable generalization capabilities when it comes to encoding ultrasound images. However, since the concept of “objectness” changes drastically in ultrasound data, we proceed to fine-tune the mask decoder - leading to ultrasound specific decoder which learns to produce contours of

objects in ultrasound. We refer to this model as SonoSAM. We demonstrate that domain-specific decoder solution, while being practical from learning perspective, is also extremely adequate from performance perspective. SonoSAM is trained on ultrasound image-mask pairs, with DiceFocal loss proposed in [24], which is linear combination of focal loss and dice loss. We utilize Adam optimizer with initial learning rate of 1e-4 and decay of 0.5 with every 25 epochs.

b) Knowledge Distillation: To enable practical utility of SonoSAM as a general purpose segmentation model for Ultrasound applications, it is desirable to have a model of a reasonable size that can be realistically deployed on devices or scanners. However, the existing foundation models trained on billions of images consume significant amount of memory and compute. To address this, in stage 2 (Fig. 2), we use knowledge distillation [30] to build a relatively light-weight student model SonoSAMLite, with SonoSAM as the corresponding teacher. The image encoder of SonoSAMLite is a lighter ViT-based architecture, resulting in a model which is 1/3rd the size of the smallest ViT-b variant. We leverage the same architecture for the other two components - prompt encoder and mask decoder. For learning, we use a weighted combination of mask loss between student and ground truth (eqn. 1), and a distribution-based distillation loss between student and teacher predictions. We use weighted loss made up of DiceFocal loss [24] as L_{mask} , and KL-Divergence loss $L_{distill}$ for our experiments, with $\alpha = 0.1$.

$$L_{student} = (1 - \alpha) * L_{mask}(\hat{y}, y) + \alpha * L_{distill}(\hat{y}, y_{SonoSAM}) \quad (1)$$

Similar to the teacher, the student model is also trained with an iterative training strategy (Section. 2.3) where prompts are iteratively sampled based on the error regions of the model predictions. We employ a best-mask distillation strategy, where the output of the teacher corresponding to the iteration reporting the best mask is used for distilling the student. We hypothesize that this allows the student model to have consistent distillation targets and ground-truth targets across iterations and enables stable learning for the student.

2.3 Iterative training mimicking user-interaction

Inspired by the success of training mechanisms presented in [18,2,3], we follow an iterative prompt selection strategy to simulate human interaction during training of both SonoSAM and SonoSAMLite. On every image, a foreground point or a bounding box is chosen with equal probability is chosen as the first prompt. For point prompt, a pixel with a controlled jitter around the foreground centroid is selected at random. Similarly, for a bounding box prompt, the box co-ordinates are altered on either side to make a loosely fitting bounding box. For both type of prompts, the maximum jitter added is around 20%. For the subsequent iterations, point prompts are uniformly sampled based on the error map between predicted mask and ground truth. Depending upon the dominant type of mistakes - false positive or false negative, a new negative or positive point is chosen in error region appropriately.

Training Data-set					
Num	Anatomy	#Images	Objects	Probe	Device
1	Fetal Heart 4ch	2500	6	2D	Voluson E8/E10
2	Fetal Heart 3VT	2120	4	2D	Voluson E8/E10
3	Fetal Thorax	8300	1	2D	Voluson E8/E10
4	Gynaecology	87000	3	3D	Voluson E10
5	Kidney	1500	1	2D	Logiq E10
6	Liver	3700	1	2D	Logiq E10
7	Bile Duct	150	1	2D	Logiq E10
8	Female Pelvic	682	1	4D	Voluson E10
9	Thyroid	800	3	2D	Logiq E10

Test Data-set					
Num	Anatomy	#Images	Objects	Probe	Device
1	Cardiac Short axis	2250	TV annulus	2D	VIVID E9/E95
2	Fetal Head	4786	HC	2D	Voluson E8/E10
3	Liver	95	Liver	2D	Logiq e
4	Breast Lesions	648	Breast lesions	3D	Public [31]
5	Musculo-skeletal	8000	Muscle tissue	2D	Public [34]
6	Nerve	3700	Brachial Plexus	2D	Public [33]
7	Adult cardiac 4ch	10000	LV, LA	2D	Public [32]
8	Adult cardiac 2ch	10000	LV, LA	2D	Public [32]

Table 1: Left: Training data-sets; Right: Test data-sets

3 Training Data-sets

Ultrasound imaging poses challenges to any AI model development, specifically for foundation models due to poor SNR and CNR compared to other imaging modalities. Moreover, the concept of “objectness” do not translate well from natural images to ultrasound. As shown on few exemplar images in Fig. 3, the object boundaries are not often well defined, texture is highly varying and overall image quality has high inter-operator variability. To build generalized foundation models, training data-set has to be curated carefully to ensure sufficient diversity. We primarily utilized data from a wide variety of commercially GE HealthCare devices for training. Our training data-set (Table. 1) includes almost 200k images with 1) varying echogenicity: Hyper-echogenic structures like fetal cranium, hypo-echogenic regions, anechoic and fluid filled objects like fetal cardiac, 2) varying interfaces: objects with soft tissue boundaries like kidney, bone-tissue interface in fetal thorax 3) varying texture: homogenous texture like liver, thyroid, and heterogeneous texture in uterus. 4) varying image quality: 2-D(convex/ sector/ linear) probes, 3-D mechanical probes and electronic 4-D probes. We demonstrate the value of curating such diverse data in results section.

4 Experiments and Results

We evaluate and report results of SonoSAM on 8 test datasets listed in Table 1. Note that these data-sets were chosen to test generalization capability of SonoSAM covering unseen anatomy (Adult Heart, Fetal Head, etc), unseen pathologies (Breast Lesions, MSK pathologies), different scanners (Logiq e), public data-sets (from different challenges). We compare the performance against



Fig. 3: Collection of images depicting variability of objects present in ultrasound.

four state-of-the-art methods namely RITM [18], FocalClick ([2]), SAM [3] and MedSAM [27]. To automatically evaluate performance of these models with increasing number of user interactions, we start with centroid of the ground truth masks and add positive negative clicks depending on evolution of predictions. We note that MedSAM [27] is not trained to work with clicks and hence we start with bounding box prompt. We use Dice Similarity Coefficient (DSC) between predicted and ground truth masks as the performance metric of choice. We report on the following set of derived metrics to analyze performance.

- Distribution of DSC scores averaged across images in each data-set versus increasing number of clicks from 1 to 10.
- NoC@80, NoC@90: Number of clicks required to achieve average dice of 80% and 90% respectively.
- Failure Rate: Fraction of images where DSC score is less than 80% and 90% DSC at NoC@80 and NoC@90 respectively.
- MaxDSC: Maximum Average DSC score after 10 clicks.

4.1 Results on 2D images

a) SonoSAM achieves state-of-the-art performance on all test datasets: SonoSAM achieves > 90% DSC on all data-sets and comfortably surpasses competing methods by a huge margin which struggle to cross even 80% DSC. As shown in Table. 2, SAM model trained on natural images, under-performs significantly on ultrasound images often being poorer than SonoSAM in range of 8 – 41% MaxDSC. Surprisingly, MedSAM which has been trained partly on ultrasound images is often the worst performer amongst all models, despite 3 of these datasets being ‘in-domain’ data-sets for MedSAM. Lack of training with clicks, severely hampers and infact deteriorates MedSAM’s performance. FocalClick model, performs reasonably on two data-sets - Liver and Fetal Head but takes lot of clicks to get to meaningful results, as shown Fig. 4.

Anatomy	Fetal Head					Liver					Cardiac LV					Cardiac LA				
	NoC80	NoC90	FR80 %	FR90 %	Max DSC	NoC80	NoC90	FR80 %	FR90 %	Max DSC	NoC80	NoC90	FR80 %	FR90 %	Max DSC	NoC80	NoC90	FR80 %	FR90 %	Max DSC
RITM [18]	4.3	5.3	2.0	4.4	0.93	7.7	11.7	1.1	14.7	0.82	8.4	14.1	1.2	24.4	0.76	9.6	14.7	3.2	31.2	0.69
FocalClick [2]	3.8	4.9	1.4	2.7	0.94	6.9	9.3	0.0	2.1	0.91	11.8	14.6	11.3	21.4	0.66	11.7	14.2	15.3	24.2	0.67
MedSAM [27]	4.1	11.6	6.2	46.1	0.75	8.6	17.6	21.1	82.1	0.72	6.7	19.1	14.1	93.2	0.69	9.4	16.6	42.1	93.3	0.63
SAM [3]	5.8	9.0	4.1	11.4	0.88	9.8	14.1	16.8	37.9	0.78	9.4	14.3	14.0	40.6	0.75	13.7	16.3	40.2	58.1	0.53
SonoSAM	1.6	2.1	1.3	2.1	0.94	2.1	5.3	0.0	3.2	0.92	2.0	4.7	0.0	0.1	0.94	2.1	4.1	0.1	0.6	0.94
SonoSAMLite	1.6	2.7	1.4	2.0	0.96	3.2	7.4	1.1	8.4	0.93	2.1	3.9	0	0	0.96	2.4	5.3	0	0	0.93

Anatomy	MSK					Nerve					Breast Lesions					Cardiac SAX				
	NoC80	NoC90	FR80 %	FR90 %	Max DSC	NoC80	NoC90	FR80 %	FR90 %	Max DSC	NoC80	NoC90	FR80 %	FR90 %	Max DSC	NoC80	NoC90	FR80 %	FR90 %	Max DSC
RITM [18]	8.7	14.2	1.4	25.5	0.78	11.8	16.8	0.7	40.5	0.70	8.9	12.2	0.9	15.4	0.78	8.3	12.0	19.0	10.8	0.79
FocalClick [2]	7.7	12.6	0.1	6.9	0.86	9.2	13.4	0.6	7.2	0.82	7.3	9.6	2.2	3.7	0.86	7.6	10.8	0.0	0.4	0.88
MedSAM [27]	12.5	19.0	43.0	87.2	0.45	10.1	18.9	0.8	86.7	0.76	2.5	9.6	2.6	35.1	0.81	5.5	16.1	160.0	62.4	0.79
SAM [3]	14.2	18.9	46.0	85.9	0.65	9.6	15.4	0.7	38.9	0.72	5.0	8.9	7.1	18.6	0.86	5.2	11.3	53.0	12.6	0.88
SonoSAM	2.9	7.1	0.1	1.1	0.92	5.1	9.5	0.4	4.0	0.90	1.9	3.7	0.0	1.4	0.94	2.3	4.1	0.0	0.0	0.95
SonoSAMLite	2.4	5.8	0.2	0.8	0.94	5.2	8.3	0.1	0.4	0.95	2.5	5.6	0.5	3.2	0.93	2.1	4.19	0.0	0.5	0.95

Table 2: Quantitative comparisons on SonoSAM and SonoSAMLite with SOTA methods on 8 anatomies from test data-sets

b) SonoSAM with 2-3 clicks outperforms SAM’s and MedSAM’s performance with 10 clicks: Fig. 4 clearly highlights the benefit of domain-specific decoder in how quickly (often 2 clicks only), SonoSAM outperforms SAM and MedSAM. As shown in Table. 2, SonoSAM achieves 80% dice in less than 2 clicks (Noc@80) on all anatomies except on the most challenging nerve data where it takes 5.1 clicks. It is also impressive that to achieve 90% dice, SonoSAM often takes 2-6 clicks (Noc@90) except on nerve data-set. In other words, SonoSAM on average reaches 90% dice within 6 clicks on almost all of the data-sets. Failure rates of SAM and MedSAM illustrate the issues with using them for medical imaging further. Except on fetal head and breast lesions, SAM fails to achieve 90% dice on at least 40% of the images (FR@90)- which means that in roughly half the images, SAM will not provide satisfactory object contour even after 10 clicks. Failure rates of SonoSAM (FR@90) are often less than 1% except liver (3%) which means that it works on almost all types of images, making it as a generic, reliable tool for fast annotation on ultrasound images.

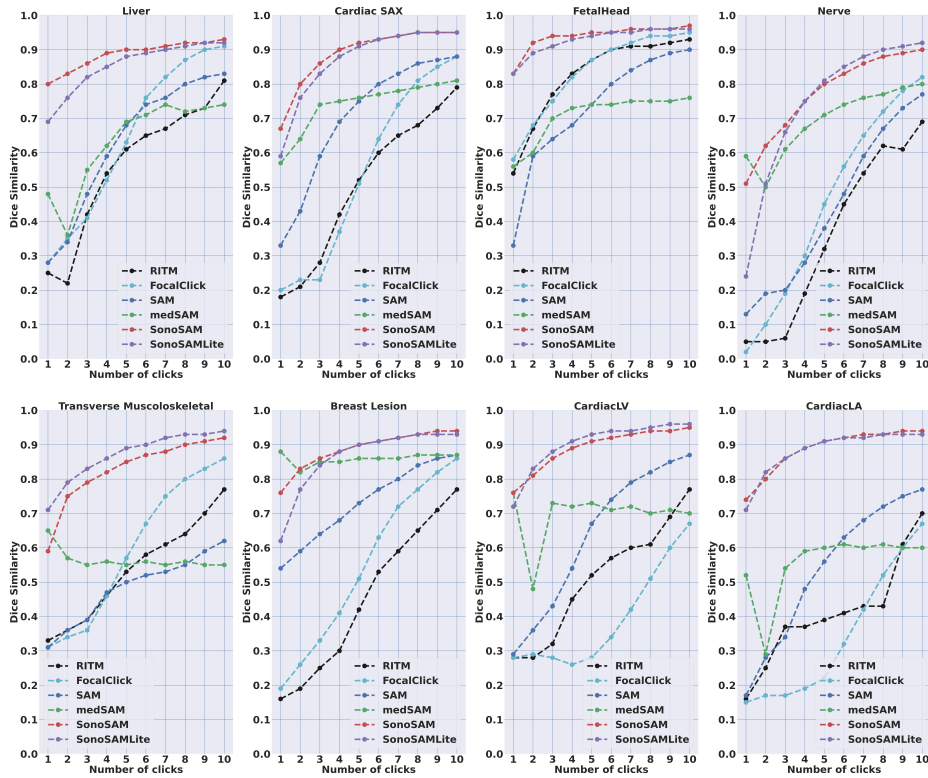


Fig. 4: Figure showing Average DSC value for SonoSAM and SonoSAMLite models along with SOTA methods for increasing number of clicks on 8 test data-sets.

c) SonoSAM behaves predictably with user interaction One of the complaints with SAM model is that, the mask generated with user clicks (positive or negative clicks) are unintuitive and unpredictable. As shown in Fig. 5, SAM often picks the entire FOV as the object and is unresponsive to multiple clicks. In contrast, SonoSAM’s responses are predictable, as demonstrated by smooth progression of predicted contours (Fig. 5).

4.2 Performance comparison of SonoSAM vs SonoSAMLite

As shown in Fig. 4, SonoSAMLite model performs very close to SonoSAM model on almost all of the 8 anatomical datasets for 1-10 clicks. For specific applications, ex. MSK and Nerve segmentation, it is quite encouraging to note that SonoSAMLite model outperforms the SonoSAM model. For a few anatomies ex. Fetal Head and Liver, the SonoSAMLite model lags slightly in the initial few clicks, however the maximum DSC at the end of 10 clicks is very similar. Likewise, as shows in Table. 2, NoC80, NoC90, FR80, FR90, Max DSC for SonoSAMLite model are very similar to SonoSAM model and shows that there is no deterioration in model performance. These results are extremely encouraging, considering that the distilled model is 1/3 rd the size of the SonoSAM model (28M parameters versus 90M parameters). The distilled model with no significant reduction in performance can have significant clinical impact and makes the usability of our work much more practical.

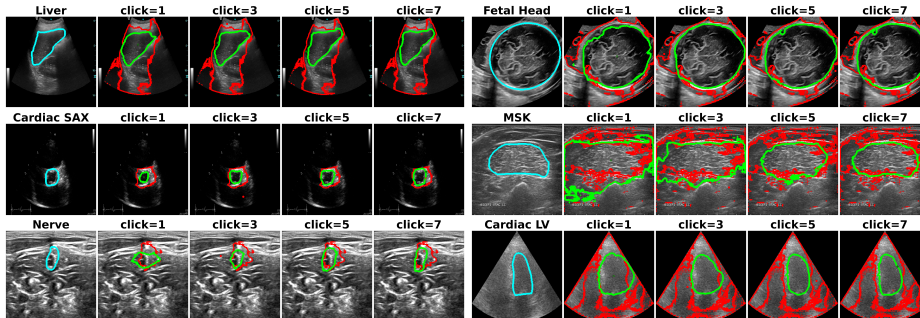


Fig. 5: Evolution of segmentation predictions for clicks - 1, 3, 5, 7 on 6 anatomies from test data-set. Legend - Red: SAM prediction, Green: SonoSAM, Cyan: GT

4.3 Evaluation on 2-D+t use-cases

Despite its practical significance, application of medical foundational models to 3-D has not receive much attention. In this section, we present initial results of our evaluations of SonoSAM for automated loop-level object segmentation. The evaluation protocol is as follows: On the first frame, we invoke SonoSAM and generate satisfactory contours for all objects. On subsequent frames, we utilize a recent SOTA tracking algorithm presented in [35] to track the objects. The deAoT method presented in [35] proposes an effective method of hierarchical propagation for video object segmentation. From independent experiments, we

found this method to work well on ultrasound images. We closely monitor the DSC overlap with ground-truth and invoke SonoSAM only when DSC falls below 90% - similar to how expert will intervene when contours have to be adjusted. We report on 3 key metrics: 1) Average Number of interventions per loop: on how many frames DSC dropped below 90%, 2) Average drop in dice per intervention: how poor was tracking when it failed 3) Average number of clicks per frame: effort required by expert to annotate entire loop.

We study the utility on tracking Left Atrium and Ventricle on 2-chamber and 4-chamber cardiac cine acquisitions with average number of frames varying around 20. The proposed framework is shown in Fig. 6. On the first frame, SonoSAM is invoked to get contours of structures of interest. On subsequent frames, the deAoT tracking algorithm is called and results are monitored. Whenever, the tracked contour’s dice overlap with ground truth is less than 90%, intervention with SonoSAM is performed to provide corrective clicks until satisfactory contours are again achieved. The process is repeated until the end of the frames. As mentioned earlier, metrics defined earlier that count number of interventions, quality of tracking at interventions and overall average number of clicks are reported. Table. 3 reports quantitative performance on these metrics averaged across 30 subjects. The key take-aways are as follows:

- The average number of interventions per loop is < 2 , which means that proposed tracking framework produces acceptable contours on all frames but 2 in the cine-loops.
- The average drop in dice before interventions is $< 2\%$, which means that even on frames where dice overlap does not exceed 90%, the drop is not significant with only 2% poorer.
- The average number of clicks per loop is ~ 1 , which is hugely significant. Roughly on a loop with 20 frames, user is expected to click only 20 times, proving the utility of the proposed approach.

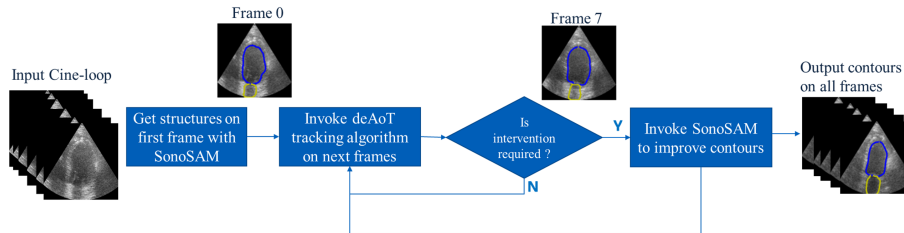


Fig. 6: Tracking framework for obtaining loop-level multi-structure segmentations using combination of SonoSAM and deAoT [35] tracking algorithm.

Qualitative results are shown in Fig. 7 and 8. These figures show start and end frames of the cine-loops for both 2 chamber and 4 chamber views. Additionally, the frames on which interventions were required (i.e.) when tracked contour’s dice

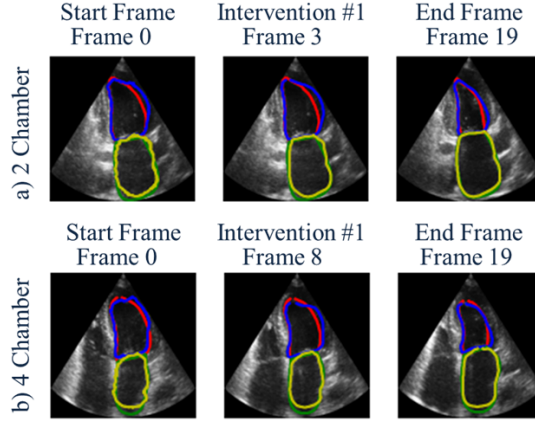


Fig. 7: Tracking results on Patient 7 with SonoSAM and deAoT [35] a) On 2-chamber u/s cine-loop b) On 4-chamber u/s cine-loop for structures Left Atrium and Left Ventricle. Apart from start and end frames, the frame at which intervention with SonoSAM was required where tracking performance decreased below 90% is shown. Legend: 1) Ground-truth a) Red: Left Ventricle b) Left Atrium 2) Prediction a) Blue: Left Ventricle b) Yellow: Left Atrium.

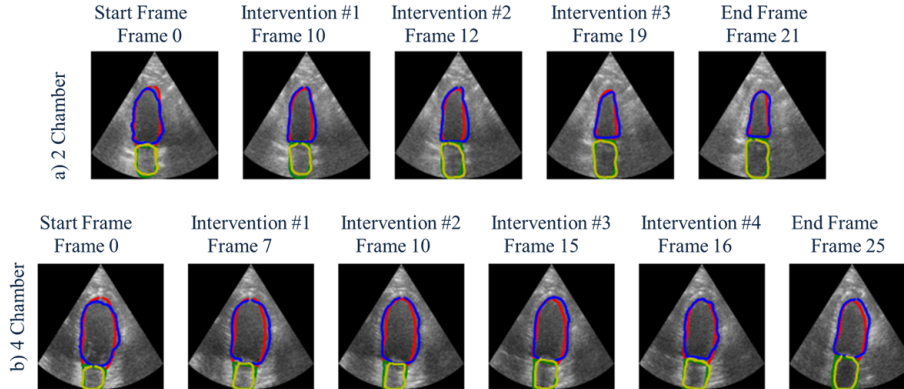


Fig. 8: Tracking results on Patient 5 with SonoSAM and deAoT [35] a) On 2-chamber u/s cine-loop b) On 4-chamber u/s cine-loop for structures Left Atrium and Left Ventricle. Apart from start and end frames, the frames at which intervention with SonoSAM was required where tracking performance decreased below 90% is shown. Legend: 1) Ground-truth a) Red: Left Ventricle b) Left Atrium 2) Prediction a) Blue: Left Ventricle b) Yellow: Left Atrium.

Anatomy/ Metric	Adult 2 Chamber		Adult 4 Chamber	
	Left Ventricle	Left Atrium	Left Ventricle	Left Atrium
Avg. num of interventions	1.7	1.2	1.9	1.4
Avg. drop of DSC before interventions	1.80%	1.30%	1.70%	1.80%
Avg. num of clicks per loop	1.1	0.9	1.0	1.0

Table 3: Quantitative results on 3 tracking metrics. Results are averaged across 30 subjects. On average, combination of SonoSAM + deAoT requires roughly 1 click per loop to get 90% or more dice overlap on all frames in the cine-loops.

falls below 90% is shown. In Fig. 7, the combination of sonoSAM and tracking was sufficient in all frames except: Frame 3. Fig. 8 depicts a tougher case, where number of interventions were three and four on 2 chamber and 4 chamber loops respectively. The averaged statistics across 30 patients are shared in Table 3.

5 Conclusion

While large vision models like SAM [3] have demonstrated extraordinary results in natural images, there have been no such models in the medical imaging world. In this work, we present SonoSAM - a breakthrough foundational model for ultrasound which for the first time - achieves performance on ultrasound images on-par with vision models in natural images. We demonstrate that by carefully curating training data-set of sufficient diversity, images in order of $200k$ is sufficient to get SOTA results. We illustrate that partial fine-tuning of large vision models - building domain-specific decoder is tractable and promising solution for ultrasound images. While success in computer vision has been achieved with humungous models, we show that with knowledge distillation, SonoSAMLite model of meager $30M$ parameters can perform as good as, if not outperform large models. In our future research, we plan to analyze failure modes in detail, explore full fine-tuning, anatomy-specific smaller models, adding text prompts and finally zero-shot segmentation.

References

1. Falk, Thorsten, et al. "U-Net: deep learning for cell counting, detection, and morphology." *Nature methods* 16.1 (2019): 67-70.
2. Xi Chen, Zhiyan Zhao, Yilei Zhang, Manni Duan, Donglian Qi, and Hengshuang Zhao. FocalClick: towards practical interactive image segmentation. *CVPR (2022)*.
3. Kirillov, A., Mintun, E., Ravi, N., Mao, H., Rolland, C., Gustafson, L., and Girshick, R. (2023). Segment anything. *arXiv preprint arXiv:2304.02643*
4. Liu, Q., Xu, Z., Bertasius, G., and Niethammer, M. (2022). SimpleClick: Interactive Image Segmentation with Simple Vision Transformers. *arXiv preprint arXiv:2210.11006*.

5. Author, A.-B.: Contribution title. In: 9th International Proceedings on Proceedings, pp. 1–2. Publisher, Location (2010)
6. LNCS Homepage, <http://www.springer.com/lncs>. Last accessed 4 Oct 2017
7. J. Bai, X. Wu, Error-tolerant scribbles based interactive image segmentation. CVPR (2014).
8. T. H. Kim, K. M. Lee, S. U. Lee, Generative image segmentation using random walks with restart. ECCV (2008).
9. S. Zhang, J. H. Liew, Y. Wei, S. Wei, Y. Zhao, Interactive object segmentation with inside-outside guidance. (CVPR) 2020.
10. J. Wu, Y. Zhao, J.-Y. Zhu, S. Luo, Z. Tu, MILCut: A sweeping line multiple instance learning paradigm for interactive image segmentation. CVPR (2014).
11. K.-K. Maninis, S. Caelles, J. Pont-Tuset, L. V. Gool, Deep extreme cut: From extreme points to object segmentation. CVPR (2018).
12. C. Rother, V. Kolmogorov, A. Blake, “GrabCut”: interactive foreground extraction using iterated graph cuts, ACM Transactions on Graphics 23 (2004).
13. Y. Boykov, M.-P. Jolly, Interactive graph cuts for optimal boundary and region segmentation of objects in n-d images. ICCV (2001).
14. L. Grady, Random walks for image segmentation. IEEE Trans. PAMI 28 (2006).
15. V. Gulshan, C. Rother, A. Criminisi, A. Blake, A. Zisserman, Geodesic star convexity for interactive image segmentation. CVPR (2010).
16. N. Xu, B. Price, S. Cohen, J. Yang, T. Huang, Deep interactive object selection. CVPR (2016).
17. Alec Radford, Jong Wook Kim, Chris Hallacy, Aditya Ramesh, Gabriel Goh, Sandhini Agarwal, Girish Sastry, Amanda Askell, Pamela Mishkin, Jack Clark, et al. Learning transferable visual models from natural language supervision. ICML (2021).
18. Konstantin Sofiiuk, Ilia A Petrov, and Anton Konushin. Reviving iterative training with mask guidance for interactive segmentation. arXiv:2102.06583 (2021).
19. S. Mahadevan, P. Voigtlaender, B. Leibe, Iteratively trained interactive segmentation. BMVC (2018).
20. Marco Forte, Brian Price, Scott Cohen, Ning Xu, and François Pitié. Getting to 99% accuracy in interactive segmentation. arXiv:2003.07932 (2020).
21. Won-Dong Jang and Chang-Su Kim. Interactive image segmentation via backpropagating refinement scheme. In CVPR, 2019.
22. Konstantin Sofiiuk, Ilia Petrov, Olga Barinova, and Anton Konushin. f-brs: Rethinking backpropagating refinement for interactive segmentation. CVPR (2020).
23. Qin Liu, Zhenlin Xu, Gedas Bertasius, and Marc Niethammer. SimpleClick: Interactive image segmentation with simple vision transformers. arXiv:2210.11006 (2022).
24. Carion, Nicolas, et al. ”End-to-end object detection with transformers.” Computer Vision–ECCV 2020: 16th European Conference, Glasgow, UK, August 23–28, 2020, Proceedings, Part I 16. Springer International Publishing, 2020.
25. Hu, E. J., Shen, Y., Wallis, P., Allen-Zhu, Z., Li, Y., Wang, S., ... and Chen, W. (2021). Lora: Low-rank adaptation of large language models. arXiv preprint arXiv:2106.09685.
26. Mazurowski, Maciej A., et al. ”Segment anything model for medical image analysis: an experimental study.” arXiv preprint arXiv:2304.10517 (2023).
27. Ma, Jun, and Bo Wang. ”Segment anything in medical images.” arXiv preprint arXiv:2304.12306 (2023).

28. Zhang, Shaoting, and Dimitris Metaxas. "On the Challenges and Perspectives of Foundation Models for Medical Image Analysis." arXiv preprint arXiv:2306.05705 (2023).
29. Zhang, Kaidong, and Dong Liu. "Customized segment anything model for medical image segmentation." arXiv preprint arXiv:2304.13785 (2023).
30. Hinton, Geoffrey, Oriol Vinyals, and Jeff Dean. "Distilling the knowledge in a neural network." arXiv preprint arXiv:1503.02531 (2015).
31. Al-Dhabyani W, Gomaa M, Khaled H, Fahmy A. Dataset of breast ultrasound images. *Data in Brief*. 2020 Feb;28:104863. DOI: 10.1016/j.dib.2019.104863.
32. S. Leclerc, E. Smistad, J. Pedrosa, A. Ostvik, et al. "Deep Learning for Segmentation using an Open Large-Scale Dataset in 2D Echocardiography" in *IEEE Transactions on Medical Imaging*, vol. 38, no. 9, pp. 2198-2210, Sept. 2019. doi: 10.1109/TMI.2019.2900516
33. Anna Montoya, Hasnin, kaggle446, shirzad, Will Cukierski, yffud, ultrasound-nerve-segmentation, Kaggle, 2016, <https://kaggle.com/competitions/ultrasound-nerve-segmentation>
34. Francesco Marzola, Nens van Alfen, Jonne Doorduyn, Kristen M. Meiburger, Deep learning segmentation of transverse musculoskeletal ultrasound images for neuromuscular disease assessment, *Computers in Biology and Medicine*, 2021, 104623, ISSN 0010-4825, <https://doi.org/10.1016/j.combiomed.2021.104623>.
35. Yang, Zongxin, and Yi Yang. "Decoupling features in hierarchical propagation for video object segmentation." *Advances in Neural Information Processing Systems* 35 (2022): 36324-36336.